Available online at www.sciencedirect.com
SCIENCE DIRECT®
Pergamon
Acta Materialia 51 (2003) 2383–2395
Acta MATERIALIA
www.actamat-journals.com

Effect of Ta on glass formation, thermal stability and mechanical properties of a $Zr_{52.25}Cu_{28.5}Ni_{4.75}Al_{9.5}Ta_5$ bulk metallic glass

G. He *, Z.F. Zhang, W. Löser, J. Eckert, L. Schultz

IFW Dresden, Institut für Metallische Werkstoffe, Postfach 270016, D-01171 Dresden, Germany

Received 3 November 2002; accepted 20 January 2003

Abstract

The effect of Ta on glass-forming ability, crystallization behavior and mechanical properties of $Zr_{52.25}Cu_{28.5}Ni_{4.75}Al_{9.5}Ta_5$ bulk metallic glass (BMG) is investigated. The solubility of Ta in the Zr-base BMG alloy depends on the arc melting conditions. 3.2 at.% Ta dissolve in the alloy inducing an increase of about 20 K in both glass transition temperature and crystallization temperature of the BMG. However, Ta does not significantly change the extension of the supercooled liquid region. The remaining Ta particles in the master alloy may induce a composition-segregation layer around the particles upon subsequent casting. This further induces the crystallization of Zr_2Cu that deteriorates the ductility of the samples. The compressive strength and ductility of the as-cast 3 mm diameter $Zr_{52.25}Cu_{28.5}Ni_{4.75}Al_{9.5}Ta_5$ samples are improved in comparison with the $Zr_{55}Cu_{30}Ni_5Al_{10}$ BMG alloy. The fracture plane of the present alloy has an angle of 31–33° with respect to the stress axis, which remarkably deviates from the maximum shear stress plane. The improvement of the mechanical properties and the peculiar fracture feature for the $Zr_{52.25}Cu_{28.5}Ni_{4.75}Al_{9.5}Ta_5$ BMG alloy can be attributed to the effect of dispersed Ta particles.

Keywords: Bulk metallic glass; Composite; Glass-forming ability; Crystallization; Mechanical properties

1. Introduction

As shown in recent comprehensive studies on bulk metallic glasses (BMGs), the glass-forming ability, stability, phase transformations, microstructure, deformation mechanisms and mechanical properties for Zr-base BMGs are quite well understood [1–3]. The addition of elements into these BMGs usually changes (often decreases) the glass-forming ability, and can give rise to partial crystallization during solidification [4]. This may be used to improve the properties of the BMGs if the crystalline phases are ductile [5] or in nanoscale [3]. However, some elements additions may lead to the formation of intrinsically brittle intermetallic compounds, which in most cases are harmful to the ductility of the materials. When the grain size and volume fraction of intermetallic phases are larger than a critical value, the material will be very

* Corresponding author. Tel.: +49-351-4659-647; fax: +49-351-4659-541.
E-mail address: guoheifw@hotmail.com (G. He).

1359-6454/03/$30.00
doi:10.1016/S1359-6454(03)00045-4

brittle, exhibiting low strength and zero plastic strain [6–11]. For example, V, Cr, Mo, Fe and Co decrease the glass-forming ability and the crystallization temperature, T_x, and narrow the temperature interval of the supercooled liquid, ΔT_x ($\Delta T_x = T_x - T_g$; T_g is the glass transition temperature) [4], thus leading to the formation of intermetallics during casting. Only few refractory metals, such as Nb, Ta and Hf form ductile crystalline phases with Zr in BMGs according to their binary phase diagrams [12] in the case of proper composition and moderate casting conditions [13]. It is expected that the refractory metals can induce the formation of a dendritic β-Ti-type crystalline phase during solidification [5,14]. Such ductile dendrites dispersed in a glassy matrix can significantly improve the plasticity of the BMGs [5,14,15] by isolating the shear banding (a very common deformation and fracture behavior in single-phase BMGs) in small discrete inter-dendritic regions [16]. Nb has been used to form dendritic β-Zr precipitates in a glassy matrix, leading to about 6% compressive plastic strain in Be-bearing Zr-base BMGs [5] and about 3% compressive plastic strain in Be-free Zr-base BMGs [14]. Ta has been added into Zr-base BMG to synthesize a glass/Ta-rich crystalline phase composite with over 15% compressive plastic strain [17]. However, so far there are very limited data to reveal the effect of Ta on the glass transition behavior and the deformation and fracture mechanisms for Zr-base BMGs in detail. In this paper, we present samples with an in situ formed Ta particles/glassy microstructure. The effect of Ta on the glass transition behavior and the mechanical properties is investigated.

2. Experimental

An alloy with nominal composition of $Zr_{52.25}Cu_{28.5}Ni_{4.75}Al_{9.5}Ta_5$ was designed by adding 5 at.% Ta into a well known $Zr_{55}Cu_{30}Ni_5Al_{10}$ alloy, which was reported to exhibit large glass forming ability [18]. A master alloy ingot was prepared by arc melting the mixture of pure Zr, Cu, Ni, Al and Ta under a Ti-gettered argon atmosphere. Then, cast cylinders with 3 and 5 mm in diameter and 50 mm in length were prepared by induction melting and then injection casting into a copper mold in a purified argon atmosphere. For comparison, thin ribbons with a thickness of about 40 μm of the same alloy were prepared by single copper wheel melt spinning. All the ribbons and cylinders were investigated by using a Perkin-Elmer 7 differential scanning calorimetry (DSC) at a constant heating rate of 20 K/min in a flowing argon atmosphere. The DSC was also used for annealing treatment of the samples. The structure of as-cast and annealed samples was analyzed by using a Philips X-ray diffraction (XRD) with CuKα radiation. Room-temperature uniaxial compression tests were carried out by using an Instron 8562 testing machine at a strain rate of 1×10^{-4}/s. The samples with an aspect ratio of 2:1 were prepared for the compressive testing. A JEOL-JSM6400 scanning electron microscope (SEM) was used for the analysis of the as-cast morphologies and fracture features. SEM electron microprobe analysis was used to determine the average compositions of the main phases.

3. Results

3.1. Influence of the melting procedure on Ta-distribution

Due to its much higher melting temperature, Ta is difficult to mix with the Zr-base BMG alloy. For getting a homogeneous master alloy, different arc melting procedures are applied for the present study. One is directly arc melting the mixture of pure Zr, Cu, Ni, Al and Ta, and the other one is arc melting pure Zr and Ta in a first step to produce a supersaturated intermediate binary Zr-Ta alloy, followed by arc melting the mixture of the intermediate alloy and the other pure metals. We have compared the master alloys prepared by the different procedures and found no difference in Ta distribution. However, repeated arc melting significantly affects the size and the distribution of the remaining Ta particles in the master alloys. Fig. 1 shows the size and the distribution of Ta (white particles, as confirmed by electron microprobe analysis) in the master alloy. After three times arc melting, Ta

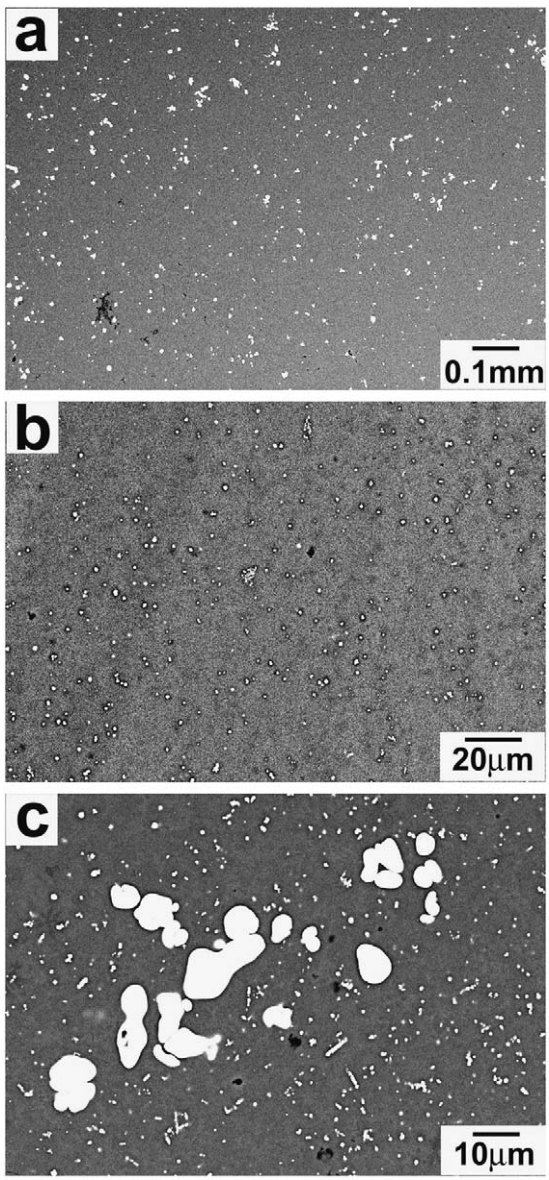

Fig. 1. Distributions of Ta in as-cast $Zr_{52.25}Cu_{28.5}Ni_{4.75}Al_{9.5}Ta_5$ master alloys subjected to different melting conditions: (a) after arc melting; remelting 3 times, (b) remelting 5 times and (c) inhomogeneously dispersed Ta after remelting 5 times.

particles with a size of about 5~20 μm are visible (Fig. 1(a)). After five times arc melting, the Ta particle size is reduced to about 0.5~1 μm (Fig. 1(b)). Some larger Ta particles can be observed in the bottom of the ingot near the water-cooled copper hearth (Fig. 1(c)). This inhomogeneous Ta-distribution can be avoided by cutting the button into pieces between each arc melting procedure. Once the Ta particles remain in the master alloy, their size and distribution keeps unchanged in melt-spun ribbons or cast bulk samples because the subsequent induction melting cannot re-melt the Ta particles.

3.2. Glass-forming ability and phase transformation

The master alloy used for producing the melt-spun ribbons was determined to contain 3.2 at.% Ta dissolved in the matrix. The remaining Ta exists in form of particles (micrograph not shown) in the as-quenched ribbons, which is indexed in the XRD pattern shown in Fig. 2(a). DSC analysis indicates that the glass transition occurs at about 705 K, and crystallization starts at about 785 K for the as-quenched ribbon, thus ΔT_x = 80 K (Fig. 3(a)). Compared to the $Zr_{55}Cu_{30}Ni_5Al_{10}$ BMG [18] (its data are also listed in Table 1), dissolution of 3.2 at.% Ta in the glass does not change ΔT_x. Ta, how-

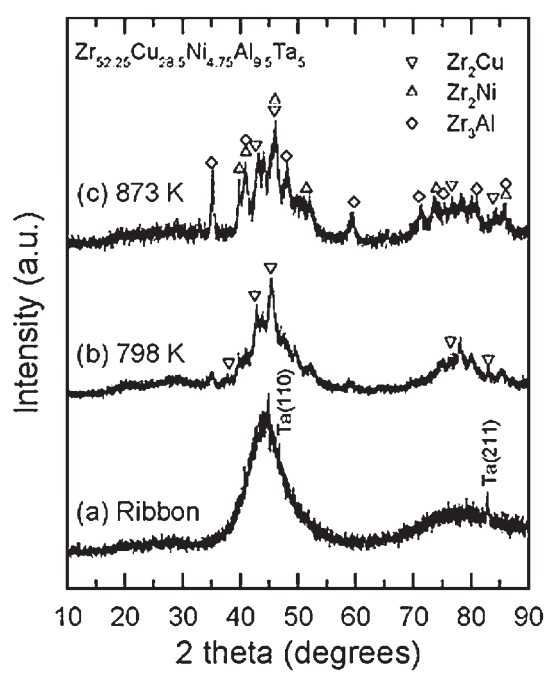

Fig. 2. XRD patterns of as-quenched and annealed $Zr_{52.25}Cu_{28.5}Ni_{4.75}Al_{9.5}Ta_5$ alloys.

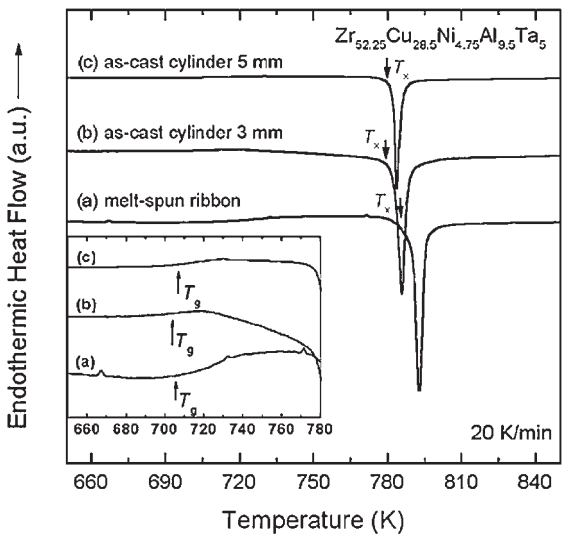

Fig. 3. DSC curves of as-cast and as-quenched $Zr_{52.25}Cu_{28.5}Ni_{4.75}Al_{9.5}Ta_5$ samples.

Table 1
Summary of glass transition temperature T_g, crystallization temperature T_x, and supercooled temperature region $\Delta T_x = T_x - T_g$ for different types of $Zr_{52.25}Cu_{28.5}Ni_{4.75}Al_{9.5}Ta_5$ samples in comparison with the data for $Zr_{55}Cu_{30}Ni_5Al_{10}$ glass

Composition (at.%)	T_g (K)	T_x (K)	ΔT_x (K)	Type of sample
$Zr_{52.25}Cu_{28.5}Ni_{4.75}Al_{9.5}Ta_5$	705	785	80	Ribbon
	703	780	77	ϕ3 mm
	708	778	70	ϕ5 mm
$Zr_{55}Cu_{30}Ni_5Al_{10}$ [18]	685	765	80	ϕ3 mm

ever, causes a shift of T_g and T_x to higher temperatures. After heating the ribbons up to 798 and 873 K, respectively, Zr_2Cu precipitates predominately at 798 K as indexed in Fig. 2(b). The stable crystalline phases consist of Zr_2Cu, Zr_2Ni and Zr_3Al after complete crystallization at 873 K as shown in Fig. 2(c).

3.3. As-cast microstructures

The size and the distribution of the Ta particles depend on the procedure used for preparation of the master alloy, and the diameter of the cast rods only affects the as-solidified matrix. This was confirmed for as-cast 3 and 5 mm rods. XRD analysis indicates that the microstructure contains a glassy phase and intermetallic Zr_2Cu besides Ta particles, as shown in Fig. 4. Comparing the main peaks of Zr_2Cu for the different samples reveal that the volume fraction of Zr_2Cu in the 3 mm diameter rod is smaller than in the 5 mm diameter rod. It is reasonable to assume that large samples (lower cooling rate during solidification) exhibit more crystalline precipitates in the glassy matrix. Because of the different volume fractions of crystalline phase formed in the matrix, the residual glass has a different composition in the 3 and 5 mm rods. This can be further represented in the DSC curves shown in Fig. 3(b) and (c). The exothermic DSC peak at 786 K for the 3 mm rod shifts by about 7 K from the peak temperature of 793 K determined for the ribbon. The exothermic DSC peak for the 5 mm rod decreases even by about 9 K from the peak temperature of the ribbon, because more Zr_2Cu precipitates in 5 mm rod compared to the 3 mm rod. The characteristic transition temperatures for the differently prepared $Zr_{52.25}Cu_{28.5}Ni_{4.75}Al_{9.5}Ta_5$ alloys are summarized in Table 1, where also the data [18] for the

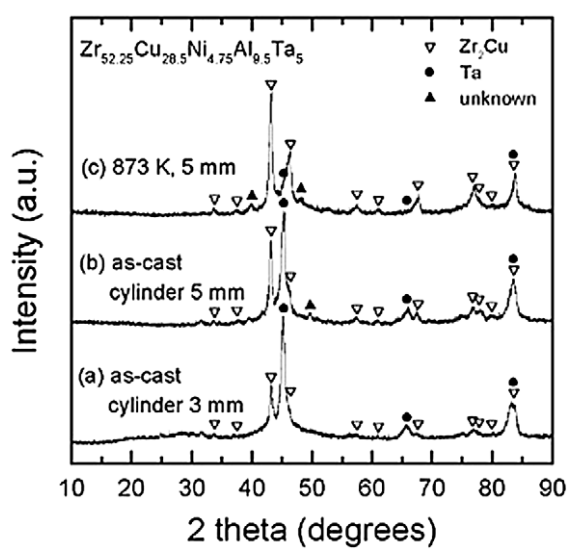

Fig. 4. XRD patterns of as-cast and annealed $Zr_{52.25}Cu_{28.5}Ni_{4.75}Al_{9.5}Ta_5$ bulk samples.

$Zr_{55}Cu_{30}Ni_5Al_{10}$ glassy alloy are listed for comparison.

Fig. 5(a) shows the as-cast microstructure of the $Zr_{52.25}Cu_{28.5}Ni_{4.75}Al_{9.5}Ta_5$ 5 mm rod. The white Ta particles dispersed in the matrix originate from the master alloy. Since the Zr_2Cu precipitates are very fine [19], their morphology and distribution in the matrix can not be revealed by SEM observation. On the other hand, an obvious contrast around the Ta particles is visible in the SEM micrographs. The composition in this area was determined by electron microprobe analysis. The inset in Fig. 5(a) shows a magnified image where a Ta particle, the area around the Ta particle and the matrix are marked by A, B and C. Electron microprobe analysis indicates that A is pure Ta, the average composition is $Zr_{51.6}Cu_{27.6}Ni_{3.0}Al_{15.8}Ta_{2.0}$ for the area B, and $Zr_{54.8}Cu_{28}Ni_5Al_9Ta_{3.2}$ for the matrix C. The Ta particles in master alloy seem to cause the formation of area B during solidification. Upon further heating the sample up to 973 K and holding there for 10 min, the Ta particles and their surrounding area on the micrograph remain unchanged (Fig. 5(b)), but a crystallization occurs in the glassy matrix (Fig. 4(c)).

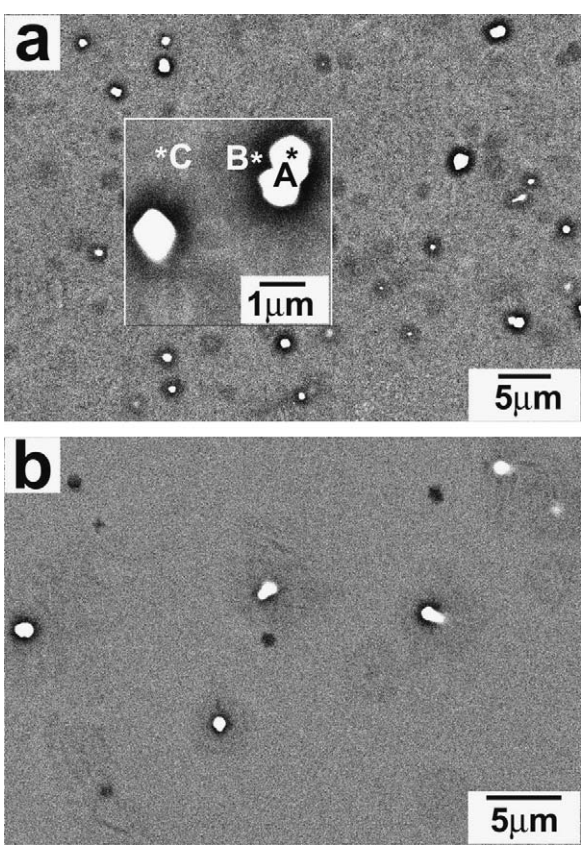

Fig. 5. Microstructure of the 5 mm diameter $Zr_{52.25}Cu_{28.5}Ni_{4.75}Al_{9.5}Ta_5$ rods: (a) as-cast state and (b) after annealing at 973 K for 10 min.

3.4. Mechanical properties of the as-cast samples

Fig. 6 shows the room temperature compressive stress-strain curves of the $Zr_{52.25}Cu_{28.5}Ni_{4.75}Al_{9.5}Ta_5$ samples with 3 and 5 mm diameter at a strain rate of $1 \times 10^{-4}s^{-1}$. For comparison, the stress-strain curve of $Zr_{55}Cu_{30}Ni_5Al_{10}$ metallic glass sample taken from reference [18] is also plotted in the figure. The $Zr_{52.25}Cu_{28.5}Ni_{4.75}Al_{9.5}Ta_5$ sample with 5 mm diameter only displays an initial elastic deformation behavior with almost no plasticity, which is quite similar to the $Zr_{55}Cu_{30}Ni_5Al_{10}$ metallic glass sample. However, the fracture strength of the present alloy is somewhat higher than that of the $Zr_{55}Cu_{30}Ni_5Al_{10}$ metallic glass, indicating a certain strengthening effect induced by the Ta particles. For the $Zr_{52.25}Cu_{28.5}Ni_{4.75}Al_{9.5}Ta_5$ sample with 3

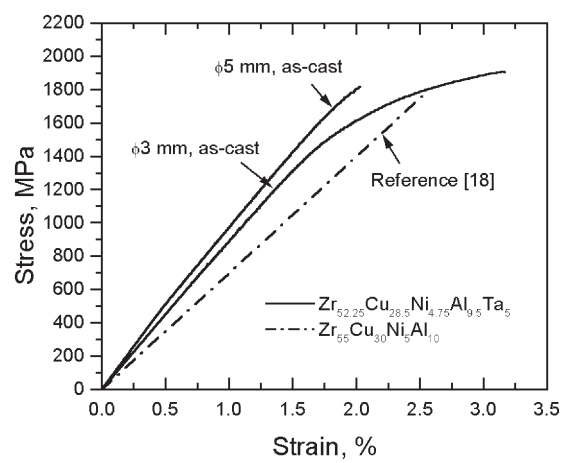

Fig. 6. Room temperature compressive stress-strain curves of $Zr_{52.25}Cu_{28.5}Ni_{4.75}Al_{9.5}Ta_5$ samples with 3 and 5mm in diameter in comparison with data for $Zr_{55}Cu_{30}Ni_5Al_{10}$ bulk metallic glass [18].

mm diameter, it is interesting to find that the alloy exhibits some distinct plasticity after elastic deformation. The sample clearly displays a strain hardening behavior and the plastic strain before failure reaches about 1.2%. Meanwhile, Young's modulus changes from 70 GPa ($Zr_{55}Cu_{30}Ni_5Al_{10}$) to 90 GPa (3 mm diameter rod) and 103 GPa (5 mm diameter rod) for the present alloy. In addition, it is noted that the fracture strength and the ductility of the present alloy strongly depend on the sample diameter or cooling conditions, i.e. the larger sample has a lower ductility. This can be explained by the difference in the volume fraction of the Zr_2Cu precipitates between the two samples. The uniaxial compressive properties for $Zr_{52.25}Cu_{28.5}Ni_{4.75}Al_{9.5}Ta_5$ are summarized in Table 2.

3.5. Fracture feature observations

SEM observations show that the fracture of the present alloy under uniaxial compressive loading always occurs in a shear mode, as seen in Fig. 7(a) and (b). The compressive fracture surface is inclined under an angle θ to the stress axis and can be measured as marked in the figures. The fracture angles θ between the stress axis and the fracture surface are equal to 31 and 33° for the two specimens with 3 mm diameter. However, the samples with 5 mm in diameter fracture to several parts after compressive test. As shown in Fig. 7(c), the fracture surface of the sample with 3 mm diameter is relatively flat and displays a typical shear fracture feature. When the fracture surface is investigated under backscattered electron contrast conditions, it is clearly seen that the white Ta particles are homogeneously distributed over the whole fracture surface, which is consistent with the observations in Fig. 1 and Fig. 5. This observation further proves that the Ta particles in the compressive sample are homogeneously dispersed in the matrix.

For most metallic glasses, it was reported that the fracture angle θ is basically along the maximum shear stress plane with an angle of 45° to the stress axis [18,20]. If the fracture angle θ is accurately measured, it was found that θ is actually smaller than 45° for the uniaxial compressive test and greater than 45° for the uniaxial tensile test. Some available data about the fracture angle θ for the uniaxial comparison are listed in Table 3 [8,21–24]. In general, θ is around 42°, but not 45°. This indicates that the compressive fracture of the metallic glasses does not exactly occur along the plane of the maximum shear stress and, consequently, does not follow the von Mises criterion [21]. However, for the present alloy, it is interesting to find that the fracture angle is only equal to 31–33°, which is markedly smaller than the common value (42°) of the fracture angle in most metallic glasses.

Further observations show that the typical feature on the fracture surfaces is a vein-like structure, as shown in Fig. 8(a) and (b). This vein-like structure is consistent with the observations in most metallic glasses [18–24]. The vein-like structure is attributed to local softening or melting within the shear band induced by the high elastic energy upon instantaneous fracture [20,23]. The soft or molten metallic glass within the shear bands easily flows and appears in a vein-like structure feature. However, in some regions on the fracture surface, we also observe another fracture feature, as shown in Fig. 8(c), which is similar to the fractography of the (nanocrystalline+glass)/dendritic crystalline composites [15] and the nanocrystalline/dendritic crystalline composites [16]. This may be attributed to the existence of the micrometer-sized Ta particles and very fine Zr_2Cu precipitates on the glass

Table 2
Summary of the compressive test data: Young's modulus E, yield stress σ_y, strain at the yield point ϵ_y, ultimate compression stress σ_{max}, and plastic strain ϵ_p

Composition (at.%)	Sample	E (GPa)	σ_y (MPa)	ϵ_y (%)	σ_{max} (MPa)	ϵ_p (%)
$Zr_{52.25}Cu_{28.5}Ni_{4.75}Al_{9.5}Ta_5$	ϕ3 mm	90	1606	1.99	1909	1.17
	ϕ5 mm	103	1721	1.87	1821	0.16

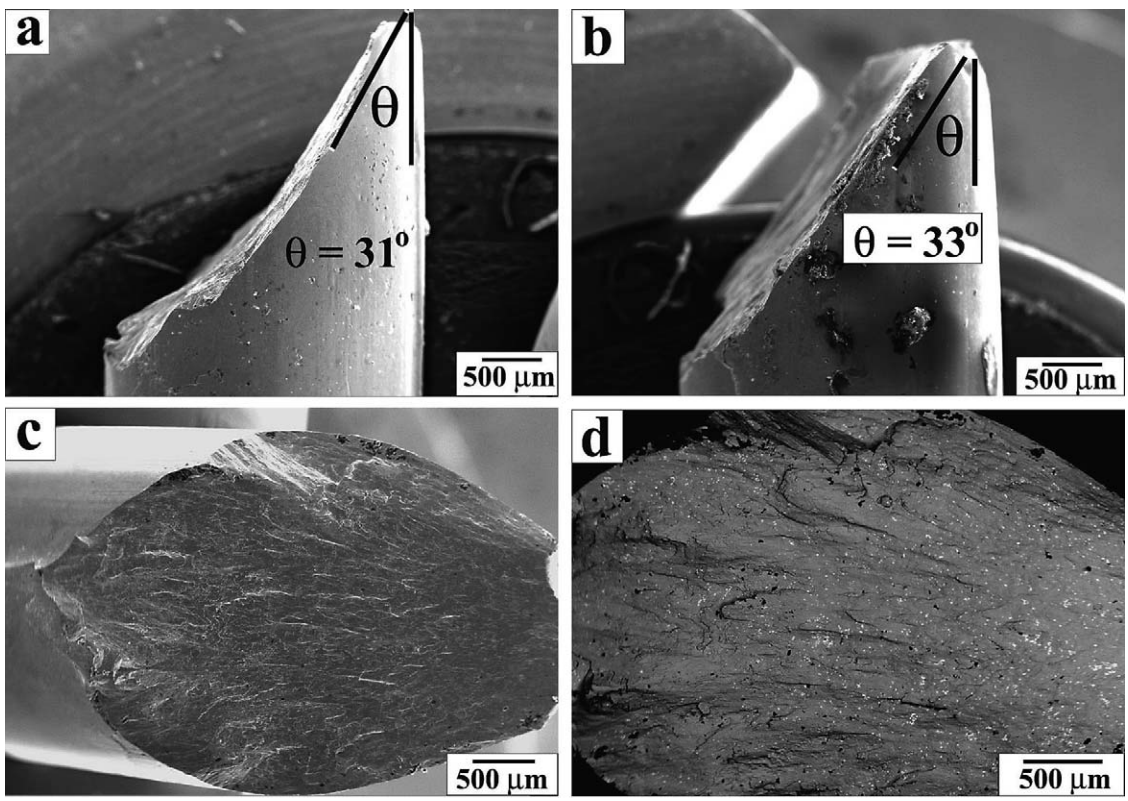

Fig. 7. Fractography of the $Zr_{52.25}Cu_{28.5}Ni_{4.75}Al_{9.5}Ta_5$ alloy under compressive loading: (a) and (b) Shear fracture behavior of the compressive samples with a shear angle of 31 and 33°. (c) Shear fracture surface morphology and (d) homogenous distribution of Ta particles on the fracture surface of the compressive samples.

Table 3
Comparison of the fracture angle θ for different BMGs

Investigators	Metallic glasses	Fracture angle (θ)
He et al. [8]	$Zr_{52.5}Ni_{14.6}Al_{10}Cu_{17.9}Ti_5$	40–45°
Donovan [21]	$Pd_{40}Ni_{40}P_{20}$	41.9 ± 1.2°
Lowhaphandu et al. [22]	$Zr_{62}Ti_{10}Ni_{10}Cu_{14.5}Be_{3.5}$	41.6 ± 2.1°
Wright et al. [23]	$Zr_{40}Ti_{14}Ni_{10}Cu_{12}Be_{24}$	42°
Zhang et al. [24]	$Zr_{59}Cu_{20}Al_{10}Ni_8Ti_3$	43°
Present result	$Zr_{52.25}Cu_{28.5}Ni_{4.75}Al_{9.5}Ta_5$	32 ± 1°

matrix. In most fracture regions, the Ta particles (marked by the arrows) can be clearly seen in the backscattered electron image, as shown in Fig. 8(d). Meanwhile, there are many regions with severe plastic deformation induced by the Ta particles, as shown in Fig. 8(e) and (f). This indicates that the Ta particles can effectively block the shear deformation of the metallic glassy matrix, and furthermore may improve the strength and possibly the ductility of the samples.

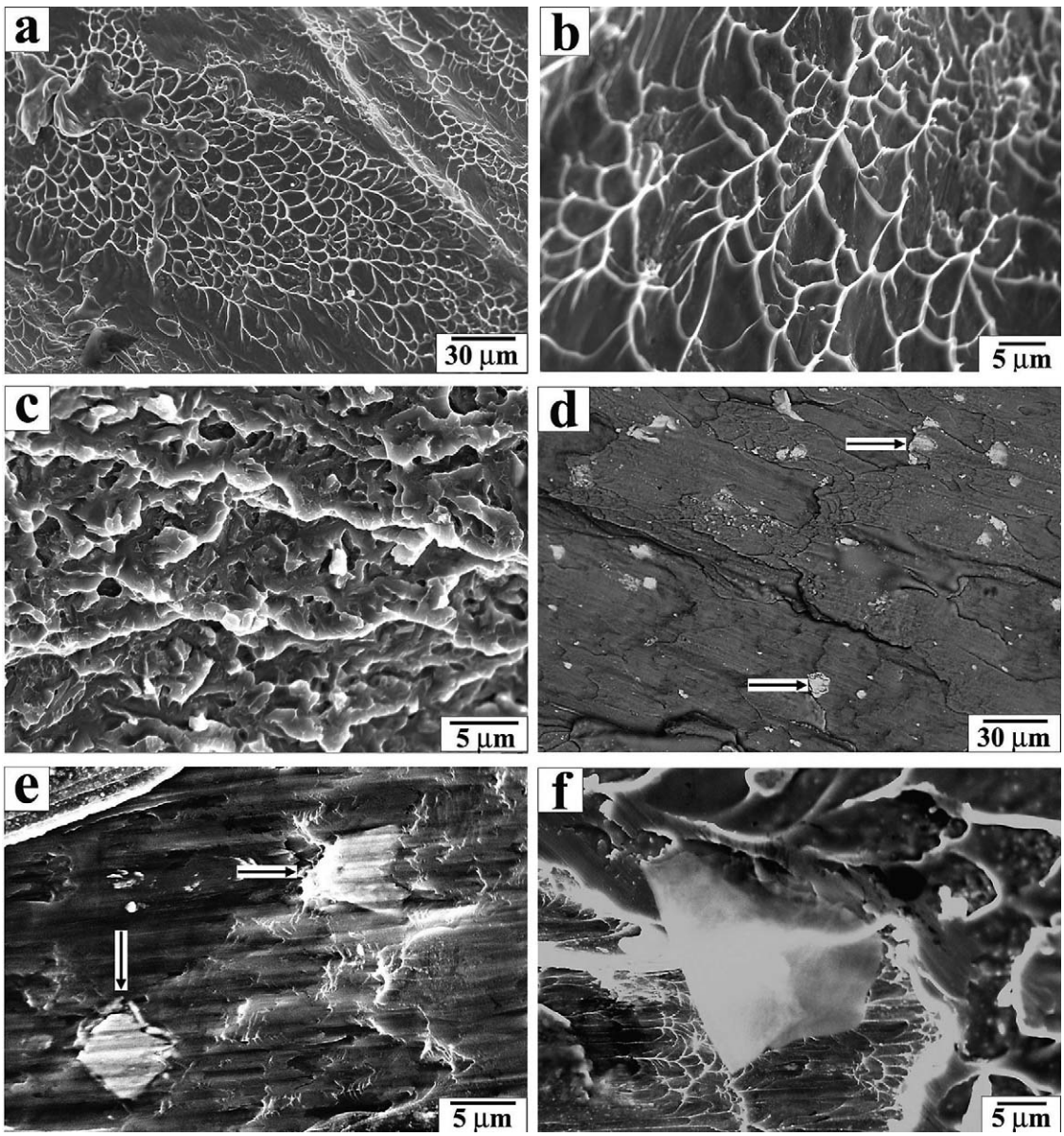

Fig. 8. Fractography of the $Zr_{52.25}Cu_{28.5}Ni_{4.75}Al_{9.5}Ta_5$ alloy under compressive loading: (a) and (b) Typical vein-like structure on the compressive fracture surfaces. (c) Fracture feature without vein-like structure at some fracture regions. (d) Distribution of Ta particles on the fracture surface. (e) and (f) Interactions of the Ta particles with the matrix glass and the Zr_2Cu precipitates under shear stress.

4. Discussion

4.1. Effect of Ta on glass-forming ability and thermal stability

The melt-spun $Zr_{52.25}Cu_{28.5}Ni_{4.75}Al_{9.5}Ta_5$ ribbon exhibits a glass transition temperature of 705 K and a crystallization temperature of 785 K at heating rate of 20 K/min. Both characteristic temperatures are about 20 K higher than those of $Zr_{55}Cu_{30}Ni_5Al_{10}$ metallic glass. About 3.2 at.% Ta causes a significant increase in stability of the glassy phase. The effect of Ta on the stability for this alloy is

consistent with that of $Zr_{59}Cu_{18}Ni_8Al_{10}Ta_5$ [25,26]. Considering that the Ta-content also leads to an increase in the melting temperature T_m of the alloy, the reduced glass transition temperature $T_{rg} = T_g / T_m$, may have a very little change in comparison with $Zr_{55}Cu_{30}Ni_5Al_{10}$ alloy. On the other hand, both the $Zr_{52.25}Cu_{28.5}Ni_{4.75}Al_{9.5}Ta_5$ and $Zr_{55}Cu_{30}Ni_5Al_{10}$ alloys exhibit a very similar supercooled liquid region ($\Delta T_x = 80$ K). This behavior is consistent with that of $Zr_{57}Nb_5Al_{10}Cu_{15.4}Ni_{12.6}$ metallic glass with addition of Ta particles [27].

For the bulk cast rods, in the case of partially precipitating intermetallic Zr_2Cu compound in the glassy matrix due to inadequate cooling rate or inhomogeneous nucleation induced by the existing crystalline particles, both the crystallization temperature, T_x, and the extension of the supercooled liquid region tend to decrease with increasing volume fraction of Zr_2Cu crystals. The lower T_x corresponds to a lower thermal stability of the glassy matrix against crystallization. This can be attributed to the changes of the composition of the glassy phase and the Zr_2Cu precipitates that may act as nucleation site to induce heterogeneous nucleation.

4.2. Effect of Ta on the as-cast microstructure and crystallization during solidification

It seems that the solubility of Ta in Zr-base BMG alloys is very different for various combinations of constituents in the alloys. Xing et al. [25] presented a very homogeneous cast microstructure for a $Zr_{59}Cu_{18}Ni_8Al_{10}Ta_5$ glass-forming alloy in which 5 at.% Ta completely dissolved into the Zr-base BMG. However, only 4 at.% Ta dissolved in the similar $Zr_{57.4}Cu_{16.4}Ni_{8.2}Al_{10}Ta_8$ BMG when a two step melting procedure was applied [17]. In present study, it is very clear that the solubility of Ta in $Zr_{55}Cu_{30}Ni_5Al_{10}$ glass-forming alloy strongly depends on the arc melting time and the homogeneity of the master alloy. After each arc melting cycle, breaking or cutting the alloy button into pieces before repeated arc melting together with long arc melting time can significantly improve the solubility of Ta and the homogeneity of the master alloy. Ta dissolved in the alloy may induce the formation of bcc-β-Ti-type solid solution dendrites during the solidification if the Zr and Ta contents are large enough. As an example, one can achieve a dendritic morphology in $Zr_{66.4}Cu_{10.5}Ni_{8.7}Al_8Ta_{6.4}$ [28]. However, when the Zr and Ta contents are lower, e.g., Zr $<$ 60 at.% and Ta $<$ 6 at.%, Ta does not induce a dendritic morphology [28]. Though no data so far show the effect of the dissolved Ta on the crystallization of BMG alloys during solidification, the precipitation of Zr_2Cu in the 3 mm-diameter rod in the present study suggests that Ta may induce crystallization in $Zr_{55}Cu_{30}Ni_5Al_{10}$, which has a very good glass-forming ability.

On the other hand, our results show obvious evidence that Ta particles can induce a composition-segregation around the particles during solidification. In contrast to W and ceramic particles [27], Ta seems to interact with the glassy matrix to generate a layer around the Ta particle. This layer may affect the precipitation of Zr_2Cu by changing the composition of the remaining liquid and act as nucleation sites. A more detailed investigation of the interfaces between the Ta particles and the matrix is necessary.

4.3. Fracture mechanism of the Zr-based alloy with Ta particles

The deformation and fracture mechanisms of BMGs have been widely investigated in the past decades [21,29–33]. It was frequently observed that the fracture of BMGs did not proceed along the maximum shear plane, no matter whether under tensile or compressive loading [20–24]. This phenomenon has been explained by taking the effect of the normal stress into account [24]. Under uniaxial compressive loading, the fracture plane often has an angle of $42-43°$ with respect to the stress axis, as listed in Table 3. However, for the present BMG composite, the fracture angle (31–33°) is obviously smaller than the common value of 42–43°, as shown in Fig. 7(a) and (b). This indicates that the fracture mechanism of the present BMG composite should be different from single-phase metallic glasses due to the interactions among the micrometer-sized Ta particles, fine Zr_2Cu precipitates and the glassy matrix. To understand the special fracture features of such com-

posites, the normal stress has been considered as important contribution for the deviation of the fracture angle from the maximum shear stress plane. Considering the critical shear fracture stress τ_C on the plane under a normal compressive stress σ, one can generally write [24]:

$$\tau_C = \tau_\theta + \mu \cdot \sigma_\theta \tag{1}$$

Here, μ is a constant of the material. For a uniaxial compressive specimen, the normal and shear stresses σ_θ and τ_θ on any plane under the uniaxial compressive loading can be easily calculated from the following equations:

$$\sigma_\theta = \sigma \cdot \sin^2(\theta) \tag{2a}$$

$$\tau_\theta = \sigma \cdot \sin(\theta) \cdot \cos(\theta) \tag{2b}$$

Here, σ is the uniaxial compressive stress. By substituting σ_θ and τ_θ into Eq. (1), one can get the critical fracture condition as below:

$$\sigma^F \geq \frac{\tau_\theta}{\sin(\theta) \cdot [\cos(\theta) - \mu \cdot \sin(\theta)]} \tag{3}$$

It is apparent that the fracture stresses, σ^F, depends on the shear angle θ. There is a minimum value of the fracture stresses at different shear angles. On the other hand, the specimens should preferentially fracture along a favorable shear plane at the minimum applied stresses. Therefore, the minimum applied fracture stresses, σ^F, must correspond to the measured fracture angles (as illustrated by Fig. 9). Thus, the following equation can be obtained:

$$\frac{\partial(1/\sigma^F)}{\partial\theta} = \frac{1}{2\tau_\theta}[\cos(2\theta) - \mu \cdot \sin(2\theta)] = 0 \tag{4}$$

From the experiments, $\theta = 42^\circ$ for the single-phase BMGs (as in Table 3), and $\theta = 32^\circ$ for present samples. Therefore, from Eq. (4), the two constants μ_{mg} and μ_{cp} for a single-phase BMGs and the present BMG composite can be calculated as follows:

$$\mu_{mg} = \left(\frac{\cos(2\theta_{mg})}{\sin(2\theta_{mg})}\right) = ctg84^\circ = 0.11 \tag{5a}$$

$$\mu_{cp} = \left(\frac{\cos(2\theta_{cp})}{\sin(2\theta_{cp})}\right) = ctg64^\circ = 0.49 \tag{5b}$$

μ_{cp} (= 0.49) is obviously larger than μ_{mg} (= 0.11), therefore, the deviation of the fracture angle from 45° is more pronounced for the composite ($\theta_{cp} = 32°$) than for the metallic glass ($\theta_{mg} = 42°$). This indicates that the normal compressive stress should play a more remarkable role in the fracture process of the present composite than the fully glassy specimen. Therefore, we can consider the two constants μ_{cp} and μ_{mg} as the structure factors of the normal stress on the shear fracture of the two materials. On the other hand, as shown in Fig. 1 and Fig. 8(d)–(f), the interactions among Ta particles, Zr_2Cu precipitates and the glassy matrix have been observed during shear fracture of the present composite. These interactions should contribute to the effect of the normal stress on the fracture processes of the specimen. Therefore, from the viewpoint of the microstructure, the constant μ_{cp} can be regarded as an external reflection of the interactions among Ta particles, Zr_2Cu precipitates and the glassy matrix during deformation. In turn, those interactions will affect the deformation mechanism of the metallic glass composite, furthermore improving its mechanical properties, such as strength and ductility. Table 4 lists the strength data for different Zr-based BMGs available so far [8,14,18,24,25,34–39]. The fracture strength of the Be-free Zr-based BMGs is only in the range of 1.45–1.80 GPa. Through a partial crystallization treatment, the fracture strength of some BMGs can

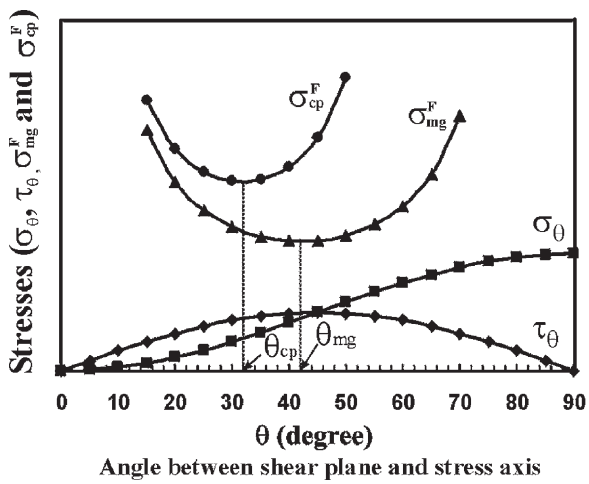

Fig. 9. Variation of the normal and shear stresses, and the fracture stresses with the fracture angle for BMG and for the BMG composite under uniaxial compressive loading.

Table 4
Comparison of fracture strength for different Zr-based BMGs

Investigators	Zr-based metallic glasses	Fracture strength (GPa)
Kawamura et al. [35]	$Zr_{65}Al_{10}Ni_{10}Cu_{15}$	1.45
Heilmaier et al. [34]	$Zr_{57}Cu_{20}Ni_8Al_{10}Ti_5$	1.60
Xing et al. [36]	$Zr_{57}Cu_{20}Ni_8Al_{10}Ti_5$	1.71 (BMG) 1.82 (Crystallization)
Zhang et al. [24]	$Zr_{59}Cu_{20}Al_{10}Ni_8Ti_3$	1.69
He et al. [8]	$Zr_{52.5}Ni_{14.6}Al_{10}Cu_{17.9}Ti_5$	1.77
Inoue et al. [37]	$Zr_{65}Al_{7.5}Ni_{10}Cu_{7.5}Pd_{10}$	1.64 (BMG) 1.83 (Crystallization)
Leonhard [18]	$Zr_{55}Cu_{30}Ni_5Al_{10}$	1.80
Fan et al. [38]	$Zr_{60}Cu_{20}Al_{10}Pd_{10}$	1.80
Kühn et al. [14]	$Zr_{66.4}Cu_{10.5}Ni_{8.7}Al_8Nb_{6.4}$	1.80
Hirano et al [39]	$Zr_{55}Cu_{30}Ni_5Al_{10}$	1.82 1.93 (with 5%ZrC) 2.00 (with 7.5%ZrC) 2.06 (with 10%ZrC) 2.14 (with 12.5%ZrC) 2.26 (with 15%ZrC)
Xing et al. [25]	$Zr_{59}Cu_{18}Ni_8Al_{10}Ta_5$	1.70
Present result	$Zr_{52.25}Cu_{28.5}Ni_{4.75}Al_{9.5}Ta_5$	1.91

be improved, but this treatment sometimes results in the disappearance of ductility [37]. However, the present BMG composite after adding Ta particles exhibits a relative high strength along with an enhanced plasticity. Combined with the other results [17,25,27,39–41], it is clear that adding crystalline particles such as Ta, W, ZrC or strong fibers into the Zr-base BMGs can change their deformation and fracture mechanism, and then can somewhat improve the fracture strength and the ductility of the BMGs.

In the present work, the effect of Ta on the phase transformation and mechanical properties of the Zr-based BMG can be illustrated as in Fig. 10. The volume fraction and the grain size of the Zr_2Cu precipitates can be controlled by the cooling conditions. In addition, the volume and the size of the Ta particles can also be adjusted by the control of composition and the melting conditions, as discussed in the sections above. When the specimens of the composite are subjected to the uniaxial compressive loading, the interactions among Ta particles, Zr_2Cu precipitates and the glassy matrix will affect the deformation and fracture mechanism in comparison with the fully glassy alloy. Fig. 8(e) and (f) show some direct interactions among the Ta particles, Zr_2Cu precipitates and the glassy matrix, and the consequent change in the fracture mode can be seen in Fig. 7(a) and (b). This indicates that these interactions have changed the constant μ of the composite and, furthermore, affect the mechanical properties. In essence, the change in fracture mode reflects the change in the microstructure of the composite, which was induced by the dissolved Ta and the Ta particles during cooling. From the present work and the results of Hirano et al. [39], it is suggested that $Zr_{55}Cu_{30}Ni_5Al_{10}$-based BMG composites can be developed as a high strength alloys with a fracture strength of more than 2 GPa together with good ductility through the addition of crystalline particles such as Ta or ZrC under an optimum microstructure condition.

5. Conclusions

1. Refractory Ta is hard to dissolve into Zr-base BMGs. The solubility of Ta depends on arc melting conditions when the Ta-content is below about 5 at.%. To improve the dissolution of Ta and its homogeneity in the Zr-base BMG, a long arc melting time is needed. The size and

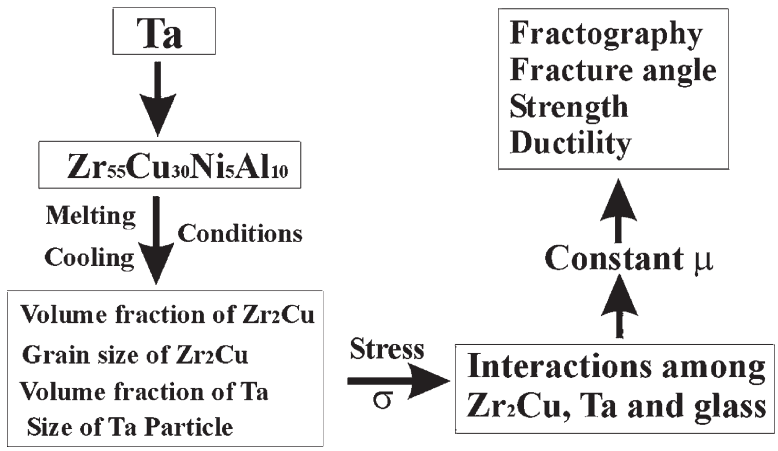

Fig. 10. Effect of Ta on phase transformation and mechanical properties of $Zr_{55}Cu_{30}Ni_5Al_{10}$ BMG composite.

the volume fraction of Ta particles present in the master alloy can be controlled by using appropriate arc melting conditions. These Ta particles can be withheld upon subsequent casting and act as a strengthening phase in Zr-base BMGs.

2. About 3.2 at.% Ta dissolved in the alloy increase T_g and T_x by about 20 K. The T_g/T_m and ΔT_x values of the Zr-base BMG alloy, however, do not change significantly. 3.2 at.% Ta only improve the thermal stability of the Zr-base BMG matrix, but do not change its glass forming ability significantly.
3. With increasing diameter of as-cast samples, the volume fraction of Zr_2Cu precipitated during solidification increases, which deteriorates the ductility of the samples. The precipitation of Zr_2Cu partially depends on the decrease in cooling rate during casting with increasing the sample diameter. The existing Ta particles can induce a composition-segregation layer around the particles, which may further lead to the crystallization of Zr_2Cu during solidification.
4. Uniaxial compression tests show that Young's modulus increases from 70 GPa ($Zr_{55}Cu_{30}Ni_5Al_{10}$) to 90 GPa (3 mm diameter rod) and 103 GPa (5 mm diameter rod) for the present alloy. The specimen with 3 mm diameter clearly displays strain hardening behavior and the plastic strain before failure reaches about 1.2%, which is higher than that of single-phase $Zr_{55}Cu_{30}Ni_5Al_{10}$ BMG. Meanwhile, the fracture plane of the $Zr_{52.25}Cu_{28.5}Ni_{4.75}Al_{9.5}Ta_5$ alloy has an angle of only 31–33° with respect to the stress axis, which is significantly lower than the typical value of 42–43° observed for single-phase BMGs. The difference in the mechanical properties and the fracture mechanisms between BMGs and the present BMG composite can be explained by the interactions among Ta particles, Zr_2Cu precipitates and the metallic glassy matrix.

Acknowledgements

The authors are grateful to M. Frey, H.Grahl, M. Gründlich, A. Güth, H-J. Klauß, U. Kühn, S. Müller-Litvanyi, S. Roth and S. Schinnerling for technical assistance and stimulating discussions. G. He and Z. F. Zhang are very grateful for the financial support of the Alexander-von-Humboldt Foundation. In addition, funding by the EU within the framework of the RTN-Network on bulk metallic glasses (HPRN-CT-2000-00033) is gratefully acknowledged.

References

[1] Inoue A. Mater Trans JIM 1995;36:866.
[2] Johnson WL. MRS Bull 1999;24:42.

[3] Inoue A. Acta Mater 2000;48:279.
[4] Inoue A, Shibata T, Zhang T. Mater Trans JIM 1995;36:1420.
[5] Hays CC, Kim CP, Johnson WL. Phys Rev Lett 2000;84:2901.
[6] Eckert J, Leonhard A, Weiss B, Heilmaier M. Mater Sci Eng 2001;A301:1.
[7] Eckert J, Kühn U, Mattern N, Leonhard A, Heilmaier M. Scripta Mater 2001;44:1587.
[8] He G, Lu J, Bian Z, Chen DJ, Chen GL, Tu GC, Chen GJ. Mater Trans 2001;42:356.
[9] Bian Z, Chen GL, He G, Hui XD. Mater Sci Eng 2001;A316:135.
[10] He G, Bian Z, Chen GL, Lu J, Chen DJ, Tu GC, Chen GJ, Hu XJ. J Mater Sci Tech 2001;17:389.
[11] Bian Z, He G, Chen GL. Scripta Mater 2002;46:407.
[12] Massalski TB, Okamoto H, Subramanian PR, Kacprzak L. Binary alloy phase diagrams, 2nd ed. William W. Scott, Jr, 1992.
[13] He G, Löser W, Eckert J, Schultz L. Mater Sci Eng 2003, (in press).
[14] Kühn U, Eckert J, Mattern N, Schultz L. Appl Phys Lett 2002;80:2478.
[15] He G, Löser W, Eckert J, Schultz L. J Mater Res 2002;17:3015.
[16] He G, Eckert J, Löser W, Schultz L. Nature Mater 2003;2:33.
[17] Fan C, Ott RT, Hufnagel TC. Appl Phys Lett 2002;81:1020.
[18] Leonhard A, Heilmaier M, Eckert J, Schultz L. Mater Res Symp Proc 1999;554:137.
[19] Baricco M, Spriano S, Chang I, Petrzhik MI, Battezzati L. Mater Sci Eng 2001;A304–306:305.
[20] Liu CT, Heatherly L, Easton DS, Carmichael CA, Schneibel JH, Chen CH, Wright JL, Yoo MH, Horton JA, Inoue A. Metall Mater Trans 1998;A29:1811.
[21] Donovan PE. Acta Metall 1989;37:445.
[22] Lowhaphandu P, Montgomery SL, Lewandowski JJ. Scripta Mater 1999;41:19.
[23] Wright WJ, Saha R, Nix WD. Mater Trans 2001;42:642.
[24] Zhang ZF, Eckert J, Schultz L. Acta Mater 2003;51:1167.
[25] Xing LQ, Li Y, Ramesh KT, Li J, Hufnagel TC. Phys Rev B 2001;64:180201.
[26] Xing LQ, Ochin P, Harmelin M, Faudot F, Bigot J, Chevalier JP. Mater Sci Eng 1996;A220:155.
[27] Choi-Yim H, Busch R, Köster U, Johnson WL. Acta Mater 1999;47:2455.
[28] He G, Löser W, Eckert J, Schultz L. unpublished data.
[29] Pampillo CA. J Mater Sci 1975;10:1194.
[30] Spaepen F. Acta Metall 1977;25:407.
[31] Argon AS. Acta Metall 1979;27:47.
[32] Leng Y, Courtney TH. J Mater Sci 1991;26:588.
[33] Huang R, Suo Z, Prevost JH, Nix WD. J Mech Phys Solid 2002;50:1011.
[34] Heilmaier M. J Mater Proc Tech 2001;117:374.
[35] Kawamura Y, Shibata T, Inoue A, Masumoto T. Appl Phys Lett 1996;69:2108.
[36] Xing LQ, Bertrand C, Dallas JP, Cornet M. Mater Sci Eng 1998;A241:216.
[37] Inoue A, Zhang T, Kim YH. Mater Trans JIM 1997;38:749.
[38] Fan C, Inoue A. Appl Phys Lett 2000;77:46.
[39] Hirano T, Kato H, Matsuo A, Kawamura Y, Inoue A. Mater Trans JIM 2000;41:1454.
[40] Choi-Yim H, Johnson WL. Appl Phys Lett 1997;71:3808.
[41] Choi-Yim H, Conner RD, Szuecs F, Johnson WL. Acta Mater 2002;50:2737.